polymer papers

Examination of the deformation of isotactic polypropylene and isotactic polypropylene/ethylene–propylene rubber blends by wide-angle X-ray scattering

H. W. Kammer and C. Kummerloewe
Department of Chemistry, University of Technology, Dresden, GDR

R. Greco, C. Mancarella and E. Martuscelli
Istituto di Ricerche su Tecnologia dei Polimeri e Reologia del CNR, Via Toiano 6, 80072 Arco Felice, Naples, Italy
(Received 15 September 1987; revised 20 November 1987; accepted 27 November 1987)

Wide-angle X-ray investigations have been carried out on isotactic polypropylene (iPP) and on isotactic polypropylene/ethylene–propylene rubber (iPP/EPR) blend fibres. The initial material has been crystallized and drawn at various temperatures using an Instron machine. The index of anisotropy I_a and the degree of orientation have been calculated from the X-ray photographs. It can be shown that drawing at $T_d = 150°C$ creates a bimodal crystal texture if the iPP/EPR blends contain 20 wt% EPR or more. The EPR prevents complete orientation of the iPP matrix crystals. This can be shown by the decreases in the index of anisotropy and degree of orientation with increasing EPR content. A bimodal crystal texture was also observed for iPP and the iPP/EPR 80/20 blend drawn at $T_d = 120°C$ immediately after neck formation. This bimodal texture disappeared during further drawing, in contrast to fibres drawn at 150°C. An oriented 'smectic' phase of iPP was observed for samples drawn at $T_d = 20°C$, whilst iPP and the blend fibres consist of oriented monoclinic α-phase crystals in all other cases. The study shows that two main deformation processes occur: deformation of the initial spherulites to a fibre structure and then plastic deformation of the oriented fibre structure.

(Keywords: isotactic polypropylene; ethylene–propylene copolymer; polymer blends; wide-angle X-ray; fibres; crystallization; mechanical drawing; anisotropy index; orientation degree)

INTRODUCTION

In a recent paper[1] the mechanical properties of isotactic polypropylene/ethylene–propylene rubber (iPP/EPR) blends have been investigated in terms of the various initial morphologies of the material. The influence of the rubber component on the plastic deformation of the initial spherulitic material into a fibrous material has been examined by means of electron microscopy.

In this study an attempt will be made to investigate the plastic deformation of these materials by means of wide-angle X-ray scattering. In particular the influence of the rubber component on the plastic deformation of the iPP matrix will be discussed.

The structural transformation processes occurring during the plastic deformation of iPP have been the subject of many papers[2–6] and different transformation mechanisms were discussed in the literature. Peterlin *et al.*[2–4] investigated the transformation of an originally spherulitic iPP structure to the fibre structure in the neck region by means of wide-angle and small-angle X-ray scattering. They proposed a model which assumes that the heat generated during the destruction of the initial lamellae brings about sufficient chain mobilization in the lamella blocks that they can rearrange to blocks with a new long period after deformation. The new long period is determined by the true temperature of drawing only. Juska and Harrison[5,6] proposed another model: the strain-induced recrystallization mechanism. Regions of the semicrystalline polymer melt under stress at the drawing temperature. This allows a large extension of the material followed by recrystallization at the drawing temperature. They also showed that the properties of the material after deformation depend only on the drawing temperature and are almost independent of the thermal history of the initial material.

In our investigation it could be shown that the drawing mechanism of the iPP/EPR blends changes at a certain drawing temperature T_i, which depends on the initial morphology of the samples and increases with the crystallization temperature of the initial material. It could be shown that below T_i the plastic deformation of the material is connected with the formation of voids and microcracks, which results in opaque fibres, and that above T_i transparent samples can be achieved[1].

The amorphous EPR component acts during the deformation process as a lubricating agent and drawing can be favoured. The present study has been carried out to explore in more detail the microstructure of samples drawn below and above T_i.

EXPERIMENTAL

The materials used in this study were isotactic polypropylene (iPP) with a weight-average molar mass of $M_w = 3.07 \times 10^5$ and a number-average molar mass of $M_n = 1.56 \times 10^4$ and an ethylene–propylene rubber (EPR)

0032-3861/88/060963-07$03.00

with a weight-average molar mass of $M_w = 1.80 \times 10^5$ and an ethylene content of 60 mol%. The isotactic polypropylene was provided by RAPRA and the ethylene–propylene rubber is produced by Montedison under the tradename Dutral C0054.

The polymers were blended by melt mixing in a Haake Rheocord instrument. After that, the material was compression moulded at 200°C and crystallized in a thermostated bath at various crystallization temperatures T_c. The procedure for sample preparation has been described in detail in a previous paper[1]. Blending ratios and crystallization temperatures of the samples investigated in this study are shown in *Table 1*.

Dumbbell specimens were cut from these materials and stretched using an Instron testing machine at a constant cross-head speed of 10 mm min^{-1} and at different temperatures T_d shown in *Table 1*. Wide-angle X-ray scattering photographs were obtained by means of a Rigaku Universal Microfocus camera using a collimator with a diameter of 10 μm. Ni-filtered Cu Kα radiation generated from a Philips X-ray generator (PW 1730/10) was used. The emission conditions were 50 kV and 20 mA. The beam was perpendicular to the drawing direction and to the surface of the fibres.

The index of anisotropy I_a and the degree of orientation α were calculated from the X-ray pattern by using the following equations:

$$I_a = \frac{A^{eq}_{(110)} + A^{eq}_{(040)} + A^{eq}_{(130)} + A^{\rho}_{(041)}}{A^{\rho}_{(110)} + A^{\rho}_{(040)} + A^{\rho}_{(130)} + A^{eq}_{(041)}} \quad (1)$$

and

$$\alpha = \frac{L_0 - L}{L_0} \times 100 \quad (\%) \quad (2)$$

In (1), $A^{eq}_{(hkl)}$ and $A^{\rho}_{(hkl)}$ are the intensities of the (*hkl*) reflections obtained from the X-ray pattern by means of radial scans in the equatorial (eq) direction and in the direction of the angle (ρ) between the equator and the (041) reflection. An automatic recording microdensitometer (Sintex AD-1 Flat Bed Microdensitometer) with a maximum resolution of 10 μm was used. In equation (2), L_0 is the diameter of the (130) reflection of the completely isotropic initial material, and L is the chord of the (130) equatorial maxima of the anisotropic fibre structure.

The X-ray investigations were carried out on fibres that had been drawn up to fibre rupture for the iPP/EPR blends crystallized at $T_c = 120$ and 132°C and drawn at $T_d = 90$ and 150°C, respectively, to investigate the influence of varying EPR contents on the final fibre structure. The influences of different thermal histories and of two different drawing temperatures on fibre formation were examined for pure iPP and the iPP/EPR 80/20 blend ($T_c = 20$, 80 and 126°C and $T_d = 20$ and 120°C).

Table 1 Blending ratios, crystallization temperatures T_c and drawing temperatures T_d of the iPP/EPR blends investigated

iPP/EPR (wt%)	T_c (°C)	T_d (°C)
100/00	132	150
95/ 5	132	150
90/10	132	150
80/20	132	150
60/40	132	150
100/00	120	90
95/ 5	120	90
90/10	120	90
80/20	120	90
60/40	120	90
100/00	20	20
100/00	80	20
100/00	126	20
100/00	20	120
100/00	80	120
100/00	126	120
80/20	20	20
80/20	80	20
80/20	126	20
80/20	20	120
80/20	80	120
80/20	126	120

RESULTS AND DISCUSSION

X-ray investigation of iPP/EPR fibres with various EPR contents drawn to fibre rupture

X-ray patterns of iPP/EPR fibres crystallized at $T_c = 132$°C and drawn at $T_d = 150$°C are shown as a function of the EPR content in *Figure 1*. The strong equatorial reflections seen in all X-ray patterns have the indices (110), (040) and (130). The reflections on the first layer line correspond to the (111) and (041) planes. The equatorial maxima on the (110), (040) and (130) rings are characteristic of fibre structure in which the *c*-axes of the monoclinic iPP crystallites are oriented parallel to the drawing direction. The *b*-axes are perpendicular to the drawing direction.

A weak meridional reflection appears in the (110) ring of the X-ray pattern of fibres containing 10% EPR and more. This weak meridional reflection results from a second distinct orientation of the iPP crystals, in which the *a*-axes of the crystallites are oriented approximately parallel to the fibre axis and the *b*-axes are oriented perpendicular to the fibre axis. Such a bimodal texture of iPP can only be observed for iPP/EPR fibres with 10% EPR or more drawn at $T_d = 150$°C. The meridional reflections are not visible in X-ray photographs of fibres drawn at $T_d = 90$°C as we can see in *Figure 2* for the iPP/EPR blend with an EPR content of 20%.

A bimodal texture of iPP crystals in hot-drawn and melt-spun fibres was also observed by Andersen and Carr[7]. They found that the meridional reflections for hot-drawn iPP fibres are single broad arcs and that only drawing above 155°C produces a bimodal crystal texture.

Seth and Kempster[8] studied the crystal texture of iPP blended with nylon-11. They found that a small amount of nylon-11 produces a much higher orientation of the iPP crystallites. Furthermore, they observed meridional reflections on the (110) rings, showing the presence of a second orientation of the iPP crystallites with their *a*-axes oriented parallel to the fibre axis.

It can be concluded from our results that in the case of iPP/EPR blends a bimodal texture of the iPP crystals can be produced in blends that contain 10% EPR or more by drawing them at high temperatures.

The indices of anisotropy I_a calculated by equation (1) for the iPP/EPR fibres crystallized at $T_c = 120$°C and drawn at $T_d = 90$°C and for fibres crystallized at $T_c = 132$°C and drawn at $T_d = 150$°C are shown in *Table 2*. The index of anisotropy is a quantity that characterizes the amount of iPP crystals oriented with their *c*-axes

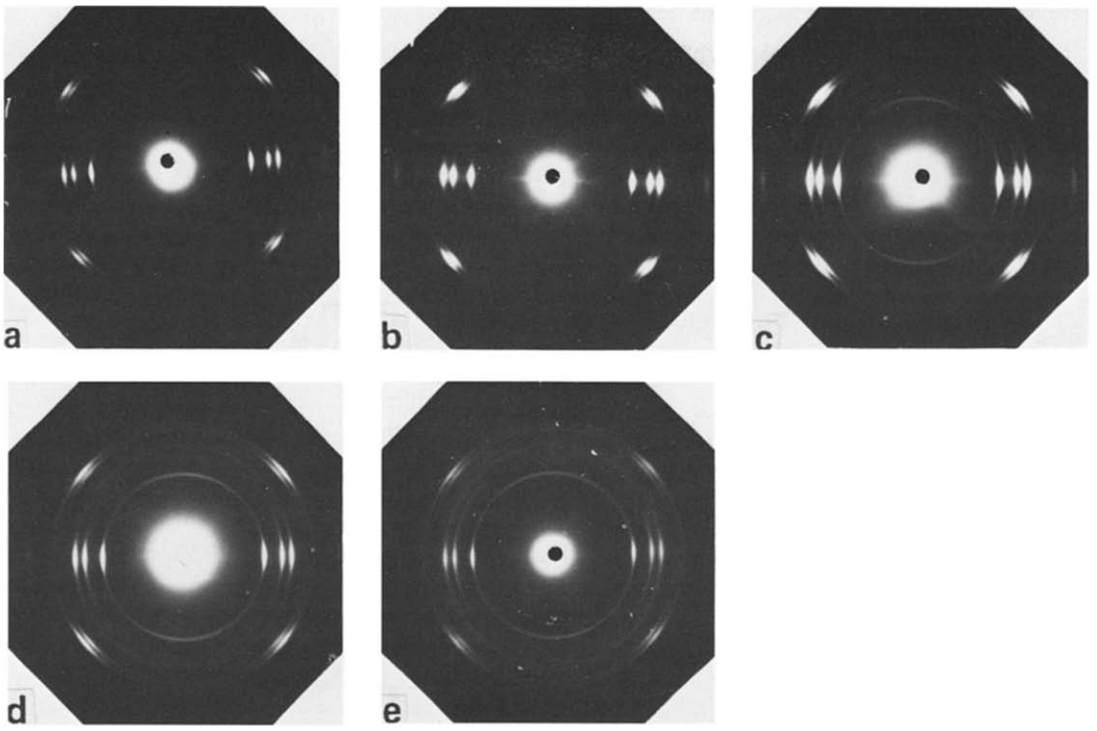

Figure 1 X-ray patterns of iPP/EPR ($T_c = 132°C$, $T_d = 150°C$) drawn up to fibre rupture. Blending ratio, iPP/EPR (wt %): (a) 100/00; (b) 95/05; (c) 90/10; (d) 80/20; (e) 60/40

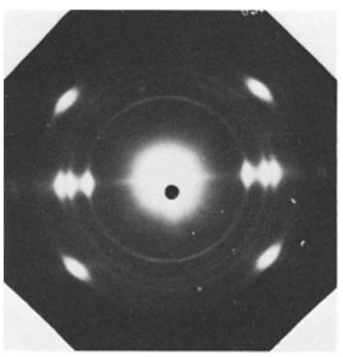

Figure 2 X-ray pattern of the iPP/EPR 80/20 fibre ($T_c = 120°C$, $T_d = 90°C$)

Table 2 Index of anisotropy I_a for iPP/EPR fibres crystallized at T_c and drawn at T_d

T_c (°C)	T_d (°C)	Composition of iPP/EPR fibres (wt %)				
		100/00	95/5	90/10	80/20	60/40
120	90	5.9	5.9	4.6	3.8	2.0
132	150	12.5	5.9	5.0	4.5	4.0

parallel to the fibre axis. Under both crystallization and drawing conditions, the index of anisotropy decreases with increasing EPR content. This means that the transformation of the initial spherulitic isotropic texture to a fibre texture of the iPP matrix will be disturbed by the EPR. A certain amount of the iPP lamellae remains unoriented. The proportion of fibrils in which the *c*-axes of the crystallites are aligned parallel to the drawing direction decreases with increasing EPR content.

Contrary to the results of Seth and Kempster[8] for iPP/nylon-11 blends, where the addition of a small amount of nylon-11 to the iPP promotes higher orientation of the iPP crystals, in our case the EPR prevents full orientation of the iPP matrix.

The index of anisotropy is much higher for the pure iPP crystallized at $T_c = 132°C$ and drawn at $T_d = 150°C$ than for the iPP crystallized at $T_c = 120°C$ and drawn at $T_d = 90°C$, but for all the blends I_a seems to be independent of T_c and T_d. From this result we can conclude that the influence of EPR on iPP orientation is much greater than the influence of thermal history and drawing conditions of the sample.

The differences in the indices of anisotropy of the pure iPP samples can only be explained in a very rough manner, because samples differ in their thermal history as well as in their drawing conditions. But if we start from the assumption that the final properties of a drawn iPP sample are chiefly governed by the drawing conditions and are independent of the initial structure, we can discuss the results as a function of the drawing temperature.

Higher drawing temperature enhances chain mobility and supports the transformation from the isotropic to the anisotropic state, which means the index of anisotropy will increase with increasing T_d. Coincidentally higher drawing temperature permits relaxation processes in the oriented amorphous phase, which influence the degree of orientation α of the crystallites. Therefore, the degree of orientation α shown in *Table 3* is higher for the fibres drawn at $T_d = 90°C$.

The degree of orientation α calculated by equation (2) is a quantity that characterizes the perfection of orientation of the *c*-axes parallel to the fibre axis. The degree of orientation is higher for the samples crystallized at $T_c = 120°C$ and drawn at $T_d = 90°C$ than for the samples crystallized at $T_c = 132°C$ and drawn at $T_d = 150°C$. The degree of orientation also decreases with increasing EPR

Table 3 Degree of orientation α for iPP/EPR fibres crystallized at T_c and drawn at T_d

T_c (°C)	T_d (°C)	Composition of iPP/EPR fibres (wt%)				
		100/00	95/5	90/10	80/20	60/40
120	90	94	94	94	85	86
132	150	88	88	81	83	81

content. According to these results the degree of orientation is influenced by both the crystallization and drawing conditions and the blending ratio.

X-ray investigation of iPP and iPP/EPR 80/20 blend crystallized at various temperatures and drawn at 20 or 120°C

Here iPP and an iPP/EPR blend with blending ratio 80/20 (wt%) were studied in terms of the thermal history of the samples before drawing and under different drawing conditions (see *Table 1*). The stress–strain plots of iPP and the blend are depicted in *Figures 3* and *4*. The drawing mechanism includes neck formation, neck propagation through the sample and a strain-hardening region. The pure iPP crystallized at $T_c = 126$°C is brittle at low drawing temperatures, as is the iPP/EPR 80/20 blend crystallized at $T_c = 80$ and 126°C. These samples tend to break before or immediately after yielding.

X-ray photographs have been taken from samples drawn until the following characteristic points of the stress–strain curve:

(a) the initial material,
(b) after neck formation,
(c) at the maximum natural draw ratio, and
(d) at fibre rupture.

The points are indicated in the stress–strain plots.

A set of X-ray photographs is shown in *Figure 5*. The samples were crystallized at $T_c = 80$°C. The iPP shown on the left side of *Figure 5* was drawn at $T_d = 20$ and 120°C, and the iPP/EPR blend at $T_d = 120$°C. The initial material is completely isotropic. The (110), (040), (130) and (111)(041) reflection rings are visible in the X-ray photographs. Therefore, the initial material consists of spherulites composed of monoclinic α-phase crystals.

The X-ray photographs taken after neck formation show the beginning of fibre formation in all samples by the presence of equatorial maxima of the (110), (040) and (130) rings and the (111)(041) maxima at the first layer line.

Samples drawn at $T_d = 20$°C. Overlapping of the (110), (040) and (130) equatorial reflections appears in the X-ray photographs of the iPP drawn at $T_d = 20$°C. This is evidence for the presence of an oriented 'smectic' phase of the iPP.

A 'smectic' phase of iPP has been observed in isotropic and anisotropic iPP[4,9,10]. This phase can be obtained by rapid quenching of an iPP melt or by drawing an iPP sample to high draw ratios at room temperature[10]. The 'smectic' iPP is composed of 3_1 helices packed in parallel fashion with high order parallel to the helix axis and less order laterally[4]. The reason for the pure packing of the 'smectic' phase is the inversion of spiralization within the helix and the presence of a random packing of left-handed and right-handed helices.

The presence of a 'smectic' phase in drawn iPP indicates a complete rearrangement of the chains from a relatively ordered manner in the initial spherulitic material, which consists of monoclinic α-phase crystals, to a more random oriented state. A 'smectic' phase appears in all samples of pure iPP crystallized at $T_c = 80$°C (see *Figure 5*) and at $T_c = 20$°C and drawn at $T_d = 20$°C.

A 'smectic' phase is also observed in the iPP/EPR 80/20 blend crystallized at $T_c = 20$°C. The X-ray pattern of the iPP/EPR 80/20 blend crystallized at $T_c = 20$°C and drawn at $T_d = 20$°C until fibre rupture is shown in *Figure 6*. Besides overlapping equatorial reflections arising from the presence of the oriented 'smectic' phase of the iPP matrix, diffraction rings of the isotropic monoclinic α-phase are visible in the X-ray photograph.

It can be concluded that a certain amount of the iPP crystals remain in the unoriented initial condition and will be not influenced by the drawing process, whereas the other part, which is included in the drawing process, will be oriented and the crystal modification will be changed from a monoclinic α-phase to the 'smectic' phase.

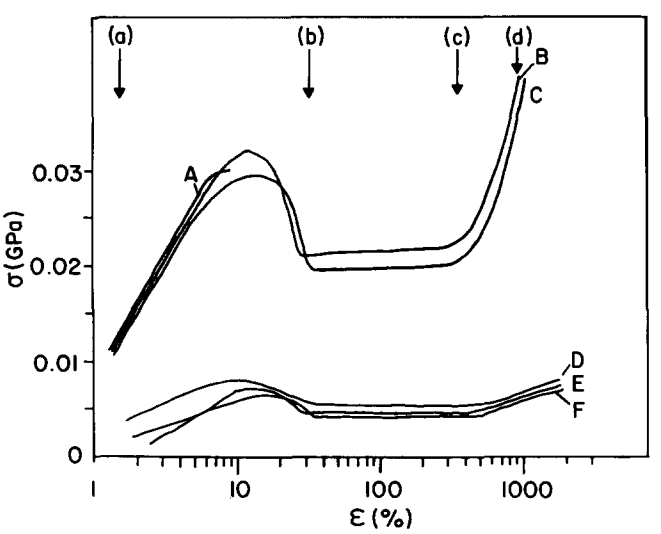

Figure 3 Stress–strain curves of iPP crystallized at T_c and drawn at T_d: A, $T_c = 126$°C, $T_d = 20$°C; B, $T_c = 80$°C, $T_d = 20$°C; C, $T_c = 20$°C, $T_d = 20$°C; D, $T_c = 126$°C, $T_d = 120$°C; E, $T_c = 80$°C, $T_d = 120$°C; F, $T_c = 20$°C, $T_d = 120$°C. The meaning of (a) to (d) is given in *Table 4*.

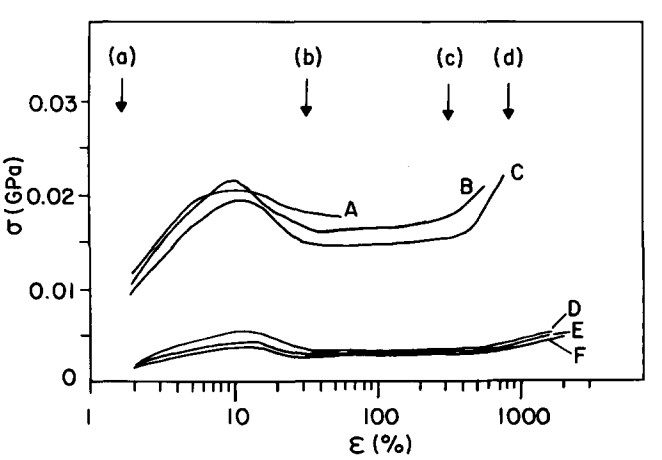

Figure 4 Stress–strain curves of iPP/EPR 80/20 blends crystallized at T_c and drawn at T_d: A, $T_c = 20$°C, $T_d = 20$°C; B, $T_c = 80$°C, $T_d = 20$°C; C, $T_c = 126$°C, $T_d = 20$°C; D, $T_c = 20$°C, $T_d = 120$°C; E, $T_c = 80$°C, $T_d = 120$°; F, $T_c = 126$°C, $T_d = 120$°C.

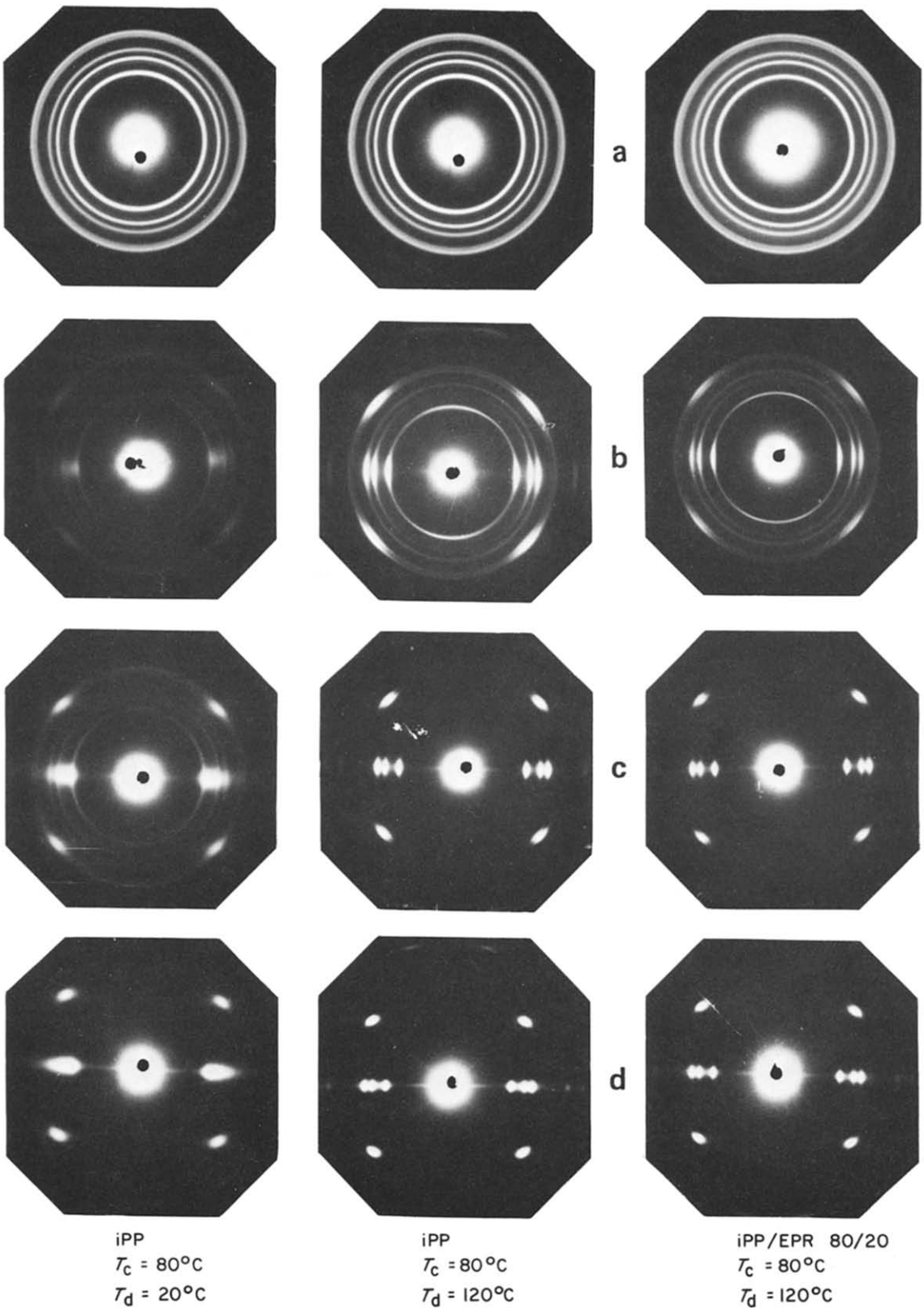

Figure 5 Wide-angle X-ray patterns of iPP crystallized at $T_c = 80°C$ and drawn at $T_d = 20$ and 120°C and of iPP/EPR 80/20 blend crystallized at $T_c = 80°C$ and drawn at $T_d = 120°C$: (a) initial undrawn material; (b) material drawn up to the formation of the neck; (c) material drawn until the natural draw ratio; (d) material drawn up to fibre rupture

Samples drawn at $T_d = 120°C$. Overlapping of the equatorial reflections disappears when the samples are drawn at higher temperatures. The characteristic reflections of the oriented α-phase crystals are visible in all X-ray patterns of fibres drawn at $T_d = 120°C$, independent of their initial morphology (see *Figure 5*).

The development of the oriented fibre structure starts in the neck region. After neck formation (*Figure 5b*), equatorial reflections of the oriented phase and reflection rings of the isotropic phase of the α-crystals are visible.

The (110) rings show a weak and broad meridional reflection for pure iPP as well as for iPP/EPR 80/20 blend

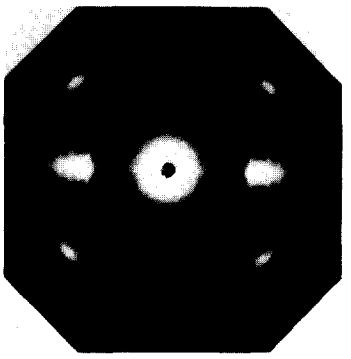

Figure 6 Wide-angle X-ray pattern of iPP/EPR 80/20 blend crystallized at $T_c = 20°C$ and drawn at $T_d = 20°C$ until fibre rupture

Table 4 Index of anisotropy I_a for iPP crystallized at T_c and drawn at T_d

		Index of anisotropy, I_a			
T_c (°C)	T_d (°C)	(a)	(b)	(c)	(d)
20	20	1.00	1.56	2.18	2.35
20	120	1.00	2.64	3.37	6.06
80	20	1.00	1.42	2.11	2.84
80	120	1.00	3.10	4.93	4.90
126	20	1.00	–	–	–
126	120	1.00	–	5.49	5.68

(a) Initial undrawn material
(b) Material drawn up to the formation of the neck
(c) Material drawn until the natural draw ratio
(d) Material drawn up to fibre rupture

drawn at $T_d = 120°C$. These meridional reflections appear only for samples drawn to complete formation of the neck. If the drawing process proceeds, the meridional reflections disappear. This means that, in the first step of the structural transformation, crystallites oriented with the *c*-axes parallel to the fibre axis as well as a small amount of crystallites oriented with *a*-axes parallel to the fibre axis exist.

In contrast to the iPP/EPR 80/20 blend drawn at 150°C discussed before (see *Figure 1d*) no *a*-axes oriented crystallites are detectable in the iPP/EPR 80/20 blend drawn at 120°C up to fibre rupture. More detailed experiments are necessary to explain the origin of the *a*-axes oriented crystals after neck formation and the mechanism of their transformation into *c*-axes oriented crystals during further drawing.

Index of anisotropy I_a and degree of orientation for iPP and iPP/EPR 80/20 blend. The indices of anisotropy I_a are shown in *Table 4* for iPP and in *Table 5* for the iPP/EPR 80/20 blend. The following conclusions can be drawn from these results:

(a) The index of anisotropy is equal to one for the initial material, i.e. the initial material is completely isotropic.

(b) I_a increases with drawing up to the natural draw ratio of the material, at which the neck has moved through the whole specimen. The structural transformation from an initial spherulitic, isotropic state to the fibre structure is finished at this point.

(c) I_a remains constant in the stress-hardening region. This means that no further orientation occurs in that region. The only exception is the pure iPP crystallized at $T_c = 120°C$, where I_a increases up to fibre rupture.

(d) The index of anisotropy is higher for iPP and the blends drawn at $T_d = 120°C$ than for those drawn at $T_d = 20°C$.

(e) The interpretation of the influence of the crystallization temperature on the index of anisotropy is not straightforward. In the case of the pure iPP, I_a seems to increase with increasing crystallization temperature if the samples are drawn at $T_d = 120°C$, whilst there seems to be no influence if one compares the two samples drawn at $T_d = 20°C$. The index of anisotropy is independent of the crystallization temperature in the case of the iPP/EPR 80/20 blends.

The degrees of orientation α of the iPP and the iPP/EPR 80/20 blend are shown in *Tables 6* and *7*. The degree of orientation increases with increasing draw ratio continuously up to fibre rupture for all specimens. There are no clear differences in the degree of orientation as a function of other parameters like crystallization and drawing temperature or blending ratio.

The α values obtained have to be discussed in connection with the index of anisotropy. The following

Table 5 Index of anisotropy I_a for iPP/EPR 80/20 blends crystallized at T_c and drawn at T_d
((a) to (d) as in *Table 4*)

		Index of anisotropy, I_a			
T_c (°C)	T_d (°C)	(a)	(b)	(c)	(d)
20	20	1.00	1.00	2.02	2.05
20	120	1.00	2.44	5.75	5.03
80	20	1.00	1.33	–	–
80	120	1.00	2.07	5.15	5.13
126	20	1.00	–	–	–
126	120	1.00	1.59	4.17	4.29

Table 6 Degree of orientation α for iPP crystallized at T_c and drawn at T_d
((a) to (d) as in *Table 4*)

		Degree of orientation, α			
T_c (°C)	T_d (°C)	(a)	(b)	(c)	(d)
20	20	0	81	89	92
20	120	0	71	88	90
80	20	0	86	82	88
80	120	0	73	88	92
126	20	0	–	–	–
126	120	0	–	86	90

Table 7 Degree of orientation α for iPP/EPR 80/20 blends crystallized at T_c and drawn at T_d
((a) to (d) as in *Table 4*)

		Degree of orientation, α			
T_c (°C)	T_d (°C)	(a)	(b)	(c)	(d)
20	20	0	0	86	90
20	120	0	75	88	90
80	20	0	0	–	–
80	120	0	77	88	91
126	20	0	–	–	–
126	120	0	76	90	91

conclusions can be drawn. Structural transformation from the spherulitic to the fibre structure may be divided into two main processes[11]. The first is deformation of the spherulites and the second is orientation of the crystallites with their *c*-axes nearly parallel to the drawing direction. The amount of crystallites oriented with their *c*-axes parallel to the drawing direction increases until the natural draw ratio of the fibres is achieved. Above the natural draw ratio the fibrillar structure will be deformed. This leads to a more perfect alignment of the *c*-axes parallel to the fibre axis and therefore to a higher degree of orientation.

ACKNOWLEDGEMENT

We thank Mr Tamburrini Arnaldo who actively contributed in carrying out densitometric measurements.

REFERENCES

1 Coppola F., Greco, R., Martuscelli, E., Kammer, H. W. and Kummerloewe, C. *Polymer* 1987, **28**, 47
2 Balta-Calleja, F. J. and Peterlin, A. *J. Polym. Sci. (A-2)* 1969, **7**, 1275
3 Balta-Calleja, F. J. and Peterlin, A. *J. Mater. Sci.* 1969, **4**, 722
4 Balta-Calleja, F. J. and Peterlin, A. *J. Polym. Sci. (A-2)* 1972, **10**, 1749
5 Juska, T. D. and Harrison, I. R. *Polym. Eng. Sci.* 1982, **22**, 766
6 Tuo-Min Liu, Juska, T. D. and Harrison, I. R. *Polymer* 1986, **27**, 247
7 Andersen, P. G. and Carr, S. H. *J. Mater. Sci.* 1975, **10**, 870
8 Seth, K. K. and Kempster, C. J. E. *J. Polym. Sci., Polym. Symp. Edn.* 1977, **58**, 297
9 Farrow, G. *J. Appl. Polym. Sci.* 1965, **9**, 1227
10 Wyckoff, H. W. *J. Polym. Sci.* 1962, **62**, 83
11 Peterlin, A. *J. Mater. Sci.* 1971, **6**, 490